Analytica Chimica Acta 1258 (2023) 341169

Contents lists available at ScienceDirect

Analytica Chimica Acta

journal homepage: www.elsevier.com/locate/aca

A versatile 3D printed multi-electrode cell for determination of three COVID-19 biomarkers

Franciele de Matos Morawski [a], Gustavo Martins [a], Maria Karolina Ramos [b], Aldo J.G. Zarbin [b], Lucas Blanes [c], Marcio F. Bergamini [a,**], Luiz Humberto Marcolino-Junior [a,*]

[a] Laboratório de Sensores Eletroquímicos (LabSensE), Departamento de Química, Universidade Federal do Paraná (UFPR), CP 19032, CEP 81531-990, Brazil
[b] Grupo de Química de Materiais, Departamento de Química, Universidade Federal do Paraná (UFPR), CP 19032, CEP 81531-990, Brazil
[c] Laboratory for Applied Science and Technology in Health, Carlos Chagas Institute, Oswaldo Cruz Foundation (Fiocruz), Curitiba, Brazil

HIGHLIGHTS

- A fully 3D-printed six-working electrode cell is proposed for detection of biomarkers.
- The working electrodes were printed with polylactic acid and carbon black.
- Detection of three COVID-19 biomarkers is investigated, aiming to achieve the whole viral window.
- The 3D-printed set-up allowed the detection of N protein, S_{RBD} protein and anti-S_{RBD}.
- The multiplex sensors were selective to serum and saliva samples.

GRAPHICAL ABSTRACT

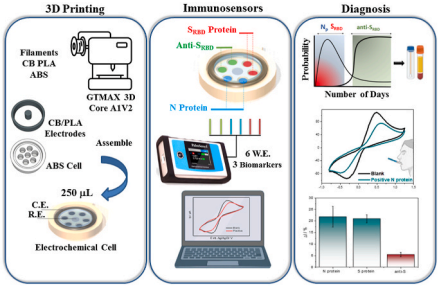

ARTICLE INFO

Handling Editor: J.P. Landers

Keywords:
3D printing
Fused deposition modelling
Multiplex
SARS-CoV-2
Immunosensors
GO

ABSTRACT

3D-printing has shown an outstanding performance for the production of versatile electrochemical devices. However, there is a lack of studies in the field of 3D-printed miniaturized settings for multiplex biosensing. In this work, we propose a fully 3D-printed micro-volume cell containing six working electrodes (WEs) that operates with 250 µL of sample. A polylactic acid/carbon black conductive filament (PLA/CB) was used to print the WEs and subsequently modified with graphene oxide (GO), to support protein binding. Cyclic voltammetry was employed to investigate the electrochemical behaviour of the novel multi-electrode cell. In the presence of $K_3[Fe(CN)_6]$, PLA/CB/GO showed adequate peak resolution for subsequent label-free immunosensing. The innovative 3D-printed cell was applied for multiplex voltammetric detection of three COVID-19 biomarkers as a proof-of-concept. The multiple sensors showed a wide linear range with detection limits of 5, 1 and 1 pg mL^{-1} for N-protein, S_{RBD}-protein, and anti-S_{RBD}, respectively. The sensor performance enabled the selective sequential detection of N protein, S_{RBD} protein, and anti-S_{RBD} at biological levels in saliva and serum. In summary, the miniaturized six-electrode cell presents an alternative for the low-cost and fast production of customizable devices for multi-target sensing with promising application in the development of point-of-care sensors.

* Corresponding author.
** Corresponding author.
E-mail addresses: bergamini@ufpr.br (M.F. Bergamini), luiz1berto@ufpr.br (L.H. Marcolino-Junior).

https://doi.org/10.1016/j.aca.2023.341169
Received 8 March 2023; Accepted 30 March 2023
Available online 3 April 2023

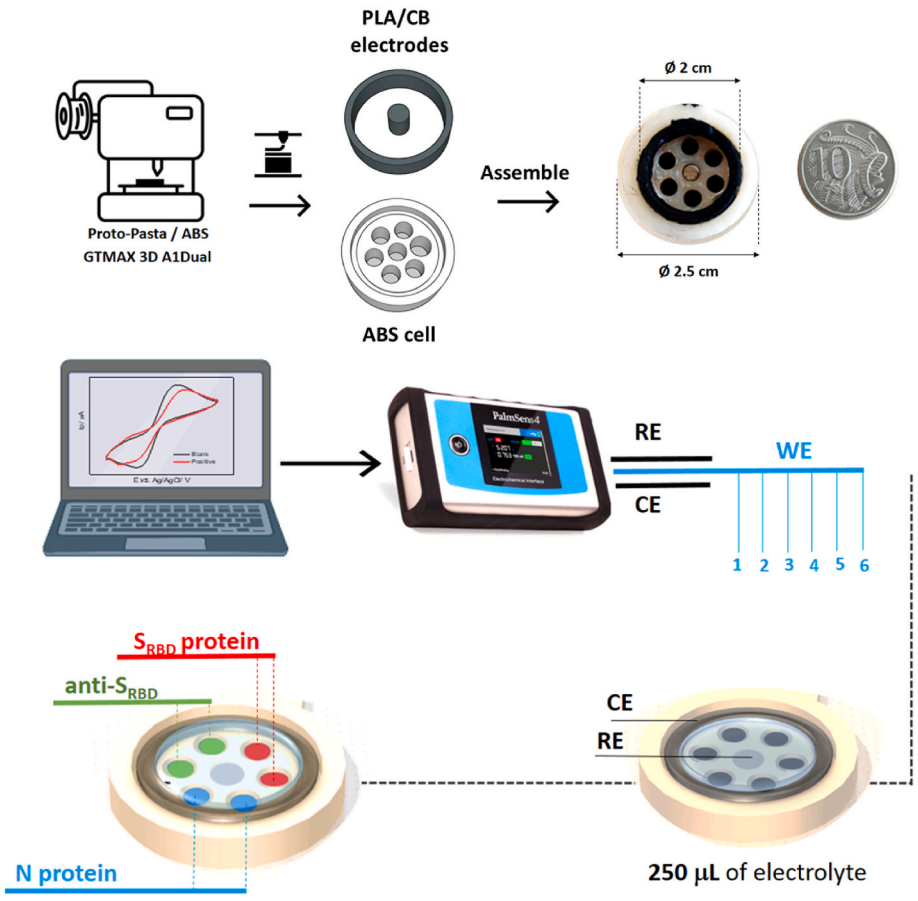

Scheme 1. Illustrative representation of the 3D-printed cell and the respective electrochemical set-up.

1. Introduction

The fused deposition modelling 3D printing technique is based on the extrusion process of thermoplastics that allows the production of three-dimensional materials using layer-by-layer deposition of conductive and/or non-conductive filaments. In electrochemistry, this breakthrough technology has shown promising applications in energy storage, microfluidic systems, and sensor devices [1–3]. From a manufacturing point of view, 3D printing is an appropriate approach for the fabrication of low-cost sensors with a capacity of production of more than 1000 electrodes/day. Moreover, additive manufacturing can be employed to create versatile and customizable electrochemical apparatus for flow-injection cells, integrated lab-on-a-chip, and wearable sensors [4–6]. It also allows the production of miniaturized electrochemical cells for portable analysis that can operate with only a few microliters of sample and supporting electrolyte [7,8]. Those characteristics are a key aspect in the development of point-of-care diagnostics ensuring operational capacity and high analytical frequency in biomedical assays.

3D-printed electrochemical sensors are commonly produced with conductive filaments of polylactic acid and carbonaceous nanomaterials [9,10]. Carbon black/polylactic acid (PLA/CB) is among the high-performance materials for conductive filaments because of its electrocatalytic properties, high surface-to-volume ratio, electrical conductivity, and low-cost. For example, the PLA/CB filaments can create electrochemical sensors with a cost of $ 0.015 dollars per electrode. Despite the low-cost and promising application, the polymeric content of 3D-printed filaments can cover the carbon conductive sites, reducing the kinetics of charge transfer onto the electrode surface. To avoid this problem, chemical and mechanical activation have been proposed in the literature as an alternative to expose the carbon sites in conductive filaments [11,12] Electrode modification with graphene oxide, and gold nanoparticles can be an additional strategy to improve the electrochemical performance and chemical functionality of PLA/CB for the production of (bio)sensors [11].

Since the beginning of the COVID-19 pandemic, multiple technologies have emerged in the field of SARS-CoV-2 detection, including colorimetric immunoassays, surface-enhanced Raman scattering, and 3D-printed electrochemical sensors. In the last few years, the use of 3D-printed technology has also emerged in the field of biosensors for electrochemical detection of Hantavirus, SARS-CoV-2 and, Influenza [13–15]. From this perspective, versatile electrochemical approaches can be employed to design multiplex sensors, contributing to a fast response with a lower sample volume. Multiplex detection can also reduce the source of experimental errors [16]. In addition, sequential or simultaneous screening of multiple biomarkers can provide more detailed information about the patient's condition, supporting medical decision-making and precision diagnostics [17]. Different geometries of miniaturized 3D-printed cells containing multiple working electrodes can be an important tool for precision medicine, ensuring the low-cost and fast production of multiplex biosensors for viral diseases [18]. From this perspective, multiplex diagnostic of SARS-CoV-2 biomarkers can improve the confidence level of COVID-19 diagnostics reducing the possibility of false negative results.

Herein, we propose a miniaturized 3D-printed electroanalytical approach containing six working electrodes coupled to a multi-channel analogical controller that operates with only 250 µL of sample. As a proof-of-concept, the novel 3D-printed cell was applied for multiplex voltammetric detection of three main COVID-19 biomarkers: N protein, S_{RBD} protein, and anti-S_{RBD} in saliva and serum samples. The analytical validation is discussed in detail in terms of linear range, accuracy, interference response and multi-target detection. The low-cost 3D-printed cell is a simple and scalable approach for accurate multiplex

electrochemical sensing.

2. Experimental

2.1. Reagents and materials

All chemical reagents were analytical grade with high purity and the solutions were prepared using distilled water. Potassium ferrocyanide, N-(3-Dimethylaminopropyl)-N′-ethylcarbodiimidehydrochloride (EDC), N-Hydroxysuccinimide sodium salt (NHS) and sodium hydroxide were purchased from Sigma Aldrich. Bovine Serum Albumin (BSA), SARS-CoV-2 receptor binding domain (S_{RBD}) 0.12 mg L^{-1}, anti-S_{RBD} protein 15.4 μg L^{-1}, Hantavirus araucaria nucleoprotein (Np) 1.18 mg mL^{-1}, anti-nucleocapsid 6.6 mg mL^{-1} (monoclonal IgG1), antigen nucleocapsid (N) 1.71 mg mL^{-1} (recombinant protein produced in E. Coli) and serum of COVID-19 patient were provided by the Molecular Virology Laboratory at Carlos Chagas Institute, FIOCRUZ/PR. The anti-S_{RBD} and anti-N standards were prepared in 10 mmol L^{-1} PBS solution in 150 mmol L^{-1} NaCl pH 7.4. S_{RBD} and N protein were diluted in 100 mmol L^{-1} TRIS buffer pH 9. A conductive filament of polylactic acid and carbon black (Protopasta) was purchased from Protoplant and employed to print the reference, working, and counter electrodes. ABS non-conductive filament was used to print the cell support and the multichannel analogical controller. GO was synthesized by hummer's method and further dispersed in water (1:5) in an ultrasonic bath for 5 min [19].

2.2. Apparatus

Scanning electron microscopy images of PLA/CB and PLA/CB/GO were obtained on a Tescan, Model: MIRA3 FEG-SEM SE, In Beam-SE, BSE detectors Coupled to OXFORD EDS detector. All images were obtained with 10 kV voltage acceleration in magnifications of 10, 25 and 50 kx. Raman spectroscopy of GO dispersion was performed in a Renishaw Microscope Imaging System 3000 coupled to an optical microscope. Thermogravimetric analysis of GO was performed in a TA Instruments equipment, Model: SDT Q600. Electrochemical measurements were provided in a potentiostat/galvanostat Palmsense 1.

2.3. 3D-printed multi-electrode cell

The multi-electrode cell was printed in a 3D CORE A1V2 printer from GTMax 3D using an extrusion nozzle with 0.4 mm of precision. The miniaturized electrochemical cell was printed with a non-conductive filament of acrylonitrile-butadiene-styrene (ABS). The geometric configuration is presented in detail in Scheme 1. The working, counter, and reference electrodes were directly printed with a commercial conductive filament of polylactic acid and carbon black (PLA/CB). The electrodes were polished with sandpaper and subsequently treated with sodium hydroxide, in order to expose the conductive portion and eliminate adsorbed contaminants in the surface, according to the previous report [20]. The reference electrode was modified with a commercial Ag/AgCl ink. Electrochemical experiments were recorded in a portable potentiostat/galvanostat Palmsense 1 (Palm Instruments B.V., the Netherlands) coupled to a laptop using PSTrace software (v. 5.4) for data acquisition. The working electrode was connected in an analogic controller coupled to the portable potentiostat with an individual output for each working electrode. This strategy ensured the sequential electrochemical determination, as presented in Scheme 1. A volume of 250 μL of $K_3[Fe(CN)_6]$ in PBS solution pH 7.4 was used as a supporting electrolyte for electrochemical measurements. Cyclic voltammetry measurements were carried out in a potential window from −0.6 to +0.8V *vs.* Ag/AgCl with a scan rate of 50 mV s^{-1}. For analytical purposes, the peak current signal was collected directly using PSTrace software. The multiple working electrodes were employed for sequential analysis of three COVID-19 biomarkers in replicate (n = 2) using two electrodes for each target. All experiments were performed at room temperature.

2.4. Preparation of the immunosensors

First, the PLA/CB was modified with GO by electrodeposition. For this purpose, an adequate volume of this dispersion was dropped in the multi-cell set-up and electrochemically deposited onto the PLA/CB surface by CV. GO electrodeposition was performed using a potential window from 0.0 to −1.7 V *vs* Ag/AgCl at 0.2 V s^{-1} for 6 scans. The produced electrodes (PLA/CB/GO) were washed with deionized water and further employed for antibody immobilization. Two PLA/CB/GO working electrodes were modified with each bioreceptors to produce electrochemical immunosensors for different SARS-CoV-2 targets: nucleocapsid protein (Np), receptor-binding domain protein (S_{RBD}), and receptor-binding domain protein IgG antibodies (anti-S_{RBD}). The electrode modification was performed by using 10 μL of a freshly prepared EDC/NHS solution (1 mg mL^{-1}), which was dropped onto the surface of each electrode on the multi-cell set-up. The electrodes were kept in contact with the solution for 45 min at 37 °C. After modification, the electrodes were rinsed with distilled water. The corresponding bioreceptor solution (2 μg mL^{-1}) was dropped onto the electrode surface, remaining at 37 °C for 45 min. BSA 0.1% (w/v) was employed to block non-specific interactions, incubated for 45 min. The resultant electrodes were named 1) BSA/anti-N/PLA/CB/GO; 2) BSA/anti-S_{RBD}/PLA/CB/GO and 3) BSA/S_{RBD}/PLA/CB/GO. For the calibration curves, 10 μL of a standard solution containing the target protein was allowed to bind at the specific receptor for 45 min at 37 °C. To adjust the concentration, protein standards were diluted in PBS 0.1 mol L^{-1} pH 7.4. The resulting electrodes were washed with deionized water and measured by CV in a potential range from −0.8 to +1.0 V vs. Ag/AgCl at 50 mV s^{-1} in the presence of 5 mmol L^{-1} $K_3[Fe(CN)_6]$ as a redox probe in PBS 0.1 mol L^{-1} pH 7.4.

2.5. Selectivity and detection in biological fluids

Since saliva samples can contain both, N and S_{RBD} proteins, their interference response was evaluated. For this purpose, 10 μL of a solution containing 50 pg mL^{-1} S_{RBD} was incubated onto BSA/anti-N/PLA/CB/GO for 45 min at 37 °C. After, CV was employed to evaluate the peak decrease. The same procedure was employed to investigate the interference of N protein onto BSA/anti-S_{RBD}/PLA/CB/GO. Another important factor of selectivity is the presence of other viral RNA expressed in saliva of a sick patient. Therefore, the influence of Hantavirus 1 ng mL^{-1} on voltammetric response was also tested aiming to evaluate the selectivity of BSA/anti-N/PLA/CB/GO and BSA/anti-S_{RBD}/PLA/CB/GO in the presence of other pathogens. For anti-S_{RBD} detection, the interference response was evaluated in the presence of COVID-19 positive and negative human serum provided by the Molecular Virology Laboratory at Carlos Chagas Institute, FIOCRUZ/PR. This experiment was performed using 10 μL of diluted serum dropped onto anti-S_{RBD}/PLA/CB/GO. Positive and negative sera dilutions in proportions of 100x, 1,000x and 10,000x were tested.

For the sequential analysis of the three targets, diluted saliva (1,000x) was spiked simultaneously with 50 pg mL^{-1} of S_{RBD} and N protein. The diluted serum sample (10,000x) was spiked with anti-S_{RBD} (50 pg mL^{-1}). A volume of 10 μL of diluted spiked saliva was dropped onto BSA/anti-N/PLA/CB/GO and BSA/anti-S_{RBD}/PLA/CB/GO. Similarly, 10 μL of diluted serum was dropped onto BSA/S_{RBD}/PLA/CB/GO. The electrochemical cell remained in contact with the samples for 45 min at 37 °C. This electrochemical set-up allows the multiplex analysis in replicate (n = 2) using two electrodes for each target in a multi-electrochemical set-up.

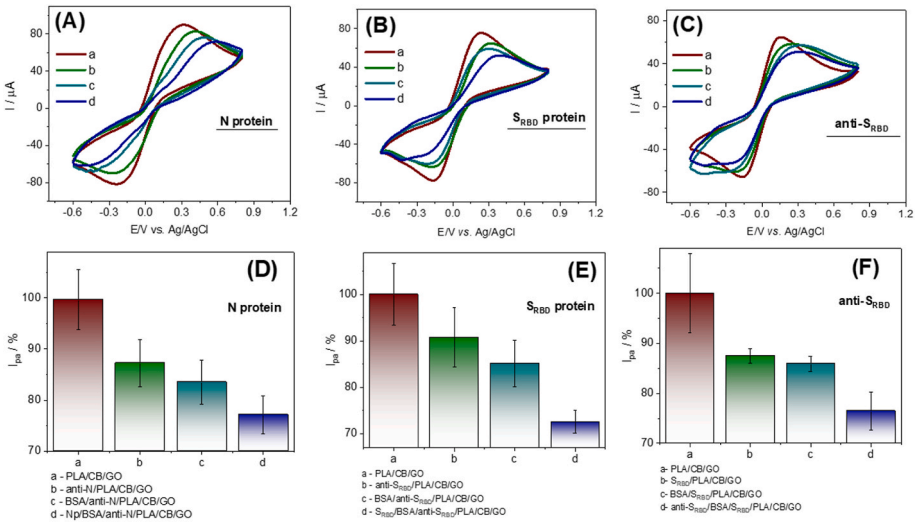

Fig. 1. Cyclic voltammetry of different biosensors produced with PLA/CB/GO in the presence of 5 mmol L^{-1} $K_3[Fe(CN)_6]$ prepared in PBS pH 7.4 for A) N-protein; B) S_{RBD} protein and C) anti-S_{RBD}; ΔI_{ap}/% of anodic peak currents stepwise monitored for D) N-protein; E) S_{RBD} protein and F) anti-S_{RBD}.

3. Results and discussion

3.1. Electrochemical performance of multi-electrode cell

The novel 3D-printed electrochemical cell set-up was designed to provide a circular symmetric geometry, as can be seen in Scheme 1. This configuration ensures that the six working electrodes are equally distributed with the same distance between the shared reference and auxiliary electrodes, providing a homogeneous charge transfer in the presence of the lowest volume of supporting electrolyte. The ring format used as an auxiliary electrode was designed to present a larger surface area, aiming to compensate the charge flow. Additionally, PLA/CB pseudo-reference electrode was coated with an Ag/AgCl ink to improve its long-term stability. The working, counter and reference electrodes were mechanically polished and chemically treated with sodium hydroxide to expose the carbon conductive sites. Scanning electron microscopy was used to characterize the PLA/CB electrodes, as can be seen in Fig. S1. Scanning electron microscopy (SEM) characterization is an important tool to investigate surface homogeneity of electrodes at a microstructural level. Since this parameter often influences sensor reproducibility, Figs. S1A and S1B show the SEM images of the PLA/CB electrodes after mechanical polishing and chemical activation, respectively. Images show a compact surface of the polished electrode, which can be attributed to coverage of carbon conductive sites with PLA. As can be seen in Fig. S1B, after chemical activation with sodium hydroxide, the increase in surface roughness suggests the apparent dissolution of PLA on the electrode surface often exposing the CB portion.

To study the adequate electrochemical operation of the multi-electrode cell, the voltammetric profile of the different six working electrodes was studied in the presence of a redox probe, as is shown in Fig. S2. For comparative purposes, the same experiment was performed in a conventional three-electrode configuration. Fig. S2A shows the voltammetric behaviour of different treated PLA/CB electrodes produced in a conventional three-electrode cell. In those conditions, the anodic and cathodic peak currents were 18.6 (±1.6) and −15.7 (±1.7) µA, respectively. The relative standard deviations of peak currents were 8.49 for I_{ap} and 10.48% for I_{pc}. In the particular case of 3D-printed six-electrode containing shared reference and counter electrodes (Fig. S2B), the peak currents were 19.9 (±0.7) and −16.3 (±1.3) with RSD values of 3.73 and 8.10% for I_{ap} and I_{cp}, respectively. This result shows that the proposed configuration allows a homogenous charge transfer and improves sensor accuracy once the measurements can be subsequently performed in the same conditions, reducing experimental source of errors. Comparing both cells, the cathodic and anodic peak potentials were also stable. The small shift in peak potential of 2 mV for E_{pa} and 7 mV for E_{pc} indicates suitable stability of the single-shared reference electrode proposed in the novel multi-electrode configuration.

3.2. Preliminaries studies

First, the optimization of voltammetric response obtained for redox probe is an important step for the fabrication of label-free electrochemical immunosensor once the proteins are commonly non-electroactive molecules, requiring indirect electrochemical detection [21]. In order to investigate the best redox probe, three aspects were evaluated for PLA/CB and PLA/CB/GO electrodes: 1) the peak current to ensure appropriate indirect detection 2) reversibility of the redox signal and 3) the sensitivity towards N protein detection. Raman spectroscopy (Fig. S3A), TGA analysis (Fig. S3B) and SEM images (Fig. S3 C, D and E) of GO used to prepare the PLA/CB/GO are showed and discussed in supplementary data.

For this purpose, two commonly used redox probes were investigated: $K_3[Fe(CN)_6]$ and hydroquinone. Figs. S4A and S4B shows the cyclic voltammetry measurements performed using PLA/CB electrode in the presence of three different concentrations of the hydroquinone and $K_3[Fe(CN)_6]$, respectively. Here, it is important to highlight that the redox probe optimization was performed in PBS solution pH 7.4, simulating biological conditions for label-free electrochemical biosensing. Despite PLA/CB (Fig. S4A) and PLA/CB/GO (Fig. S4C) present a reversible signal in hydroquinone, this probe did not show a considerable peak decrease for target protein detection, ΔI_{ap} value near to 3% (Fig. S4E). On the other hand, $K_3[Fe(CN)_6]$ was effective in the protein detection, indicating a considerable decrease of anodic peak current (ΔI_{ap} = 17%) in the presence of N protein (Fig. S4F). Thus, $K_3[Fe(CN)_6]$ in PBS 7.4 was employed for further experiments.

Since GO oxygen functional groups reduce with the increase of electrodeposition cycles, this condition was also optimized. As shown in Fig. S5, the electrochemical response of PLA/CB increases with the number of electrodeposition cycles from 1 to 12. For this purpose, the peak current difference between PLA/CB and PLA/CB/GO ($\Delta I_{ap} = I_{ap\text{-}PLA/CB/GO} - I_{ap\text{-}PLA/CB}$) was evaluated in the presence of $K_3[Fe(CN)_6]$. If compared to PLA/CB, PLA/CB/GO showed an approximately 4 and 2.5-fold increase in $K_3[Fe(CN)_6]$ in PBS 7.4 for I_{ap} and I_{cp} values, respectively. This behavior can be attributed to the increase in electroactive area and the coverage of the non-conductive PLA portion. To confirm that, the same cathodic treatment of PLA/CB was applied in PBS 7.4,

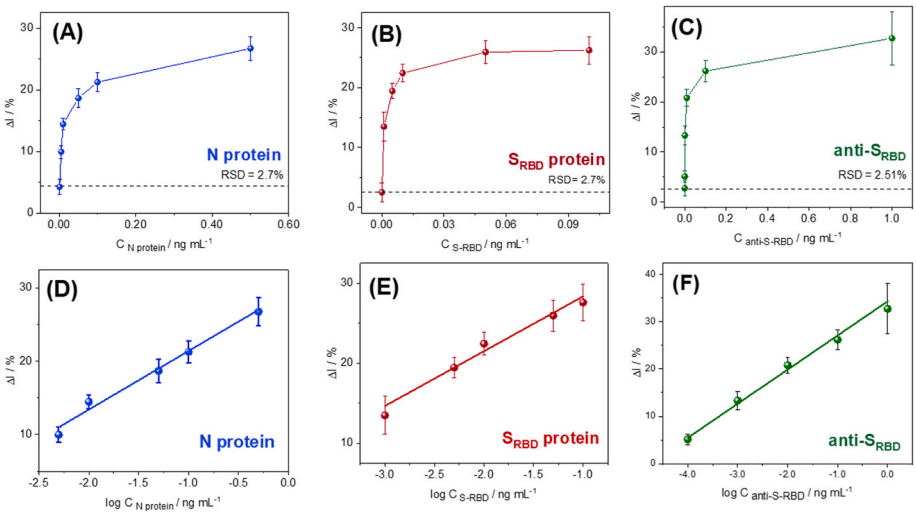

Fig. 2. Peak current variation (ΔI_{ap}/%) values obtained from CV measurements in the presence of $[Fe(CN)_6]^{3-/4}$ 5 mmol L^{-1} prepared in PBS pH 7.4 obtained for A) N-protein in a range from 5 to 500 pg mL^{-1}; B) S_{RBD} in a range from 1 to 100 pg mL^{-1}; C) anti-RBD from 1 to 1000 pg mL^{-1}; with the respective calibration plots of D) N protein; E) S_{RBD} protein and F) anti-S_{RBD}. The calibration plots were performed in PBS buffer.

providing only a slight improvement of the peak current (Fig. S5A). After 12 cycles, an apparent stabilization of the current peak indicates the effective reduction of oxygen-containing groups of GO. On the other hand, the opposite effect is observed for protein immobilization with the reduction of antibody content when more than 6 cycles of electrodeposition were applied. To evaluate that, we have studied the protein immobilization using a different number of electrodeposition cycles. This effect was estimated by the difference between the anodic peak current before and after the immobilization of N protein ($\Delta I_{ap} = I_{ap\text{-}PLA/CB/GO} - I_{ap\text{-}PLA/CB/GO/anti\text{-}Np}$). It suggests that the available oxygen groups in graphene oxide directly influence the number of available sites for protein attachment via EDC/NHS activation (Fig. S5B). As expected, those two observations are important to ensure the best electrochemical performance of biosensors. Considering that, further studies were conducted using 6 cycles of electrodeposition as the optimized condition.

3.3. Stepwise construction of the multi-target sensors

As a proof of concept, the multi-target electrochemical cell was employed in the construction of three COVID-19 sensors for the sequential detection of N-protein, S_{RBD} protein and anti-S_{RBD}. PLA/CB/GO modified electrodes were stepwise interrogated by cyclic voltammetry in a potential window of −0.6 to +0.7 V *vs.* Ag/AgCl at 50 mV s^{-1} in the presence of $K_3[Fe(CN)_6]$ prepared in PBS pH 7.4. Fig. 1A, 1B and 1C show the voltammograms provided by the different sensors: N-protein, S_{RBD} protein and anti-RBD, respectively. First, the oxygen-containing groups of PLA/CB/GO were chemically activated by EDC/NHS, as can be seen in step **a**. Subsequently, each corresponding bioreceptor (2 μg L^{-1}) was kept in contact with the activated PLA/CB/GO/EDC-NHS. Cyclic voltammograms showed a decrease in the anodic and cathodic peak currents for all testes electrodes after protein incubation (step b). The reduction in anodic peak currents ΔI_{ap} (I_{op}-I_p) were 13.7, 19.7 and 12.5% for N-protein, S_{RBD} and anti-S_{RBD} biorreceptors, respectively. This result indicates the successful protein attachment on the activated PLA/CB/GO once proteins are known to block the charge transfer reactions on the electrode/solution interface, acting as insulating layers.

Subsequently, BSA provided an I_{ap} reduction near to 5% for all electrodes (step c). This step was used to block the non-specific interactions of proteins onto PLA/CB/GO, avoiding the possible interference response. The stepwise monitoring is evidenced in Fig. 1D, 1E and 1F. Finally, the sensor was tested against each target protein. In those conditions, the reduction in ΔI_{ap} was 12.8, 15.2 and 10.1% for N-protein, S_{RBD} protein and anti-S_{RBD}, respectively. This indicates the successful detection of the three tested targets with the proposed device, providing the possible application of the multi-electrode cell for their sequential determination.

Table 1
Comparative performance of different electrochemical approaches employed to COVID-19 diagnostics.

Electrode	Method	Target	Sample	Detection time	LOD	Ref
SPE-GQD-PHB	DPV	anti-S	Serum	120 min	100 ng mL^{-1}	[24]
SPE-MWCNT	EIS	anti-S	Serum	40 min	0.7 pg mL^{-1}	[25]
AuIDE	EIS	N protein	Serum	5 min	0.389 fmol L^{-1}	[26]
SPE-CB-MBs	DPV	N protein	Saliva	30 min	8 ng mL^{-1}	[27]
FTO/AuNPs/SARS-CoV-2	DPV/CV	N protein	Saliva	120 min	0.63 fmol L^{-1}	[28]
SPE-MIP-MP-Au	EIS	S_{RBD} protein	Saliva	20 min	0.7 pg mL^{-1}	[29]
ITO-GNPs@MUA	CV/EIS	S_{RBD} protein	Swab	60 min	0.577 fg mL^{-1}	[30]
AuNP- mAB	SWV	S protein	Saliva	–	1 pg mL^{-1}	[31]
PLA/CB/GO	CV	N protein	Saliva	45 min	5 pg mL^{-1}	This work
		S_{RBD} protein	Saliva		1 pg mL^{-1}	
		anti-S_{RBD}	Serum		0.1 pg mL^{-1}	

Screen printed electrode - SPE; graphene quantum dots – GQD; Polyhydroxibutirate- PHB; multiwalled carbon nanotubes – MWCNT; gold interdigitated electrode – AuIDE; carbon black – CB; magnetic beads – MB; fluorine tin oxide – FTO; gold nanoparticles – AuNPs; molecularly imprinted polymer – MIP; macroporous gold – MP-Au; indium tin oxide – ITO; gold nanoparticles – GNPs; 11-mercaptoundecanoic acid – MUA; polylactic acid – PLA; graphene oxide – GO. Differential Pulse Voltammetry - DPV; EIS – Electrochemical Impedance Spectroscopy; CV – Cyclic Voltammetry.

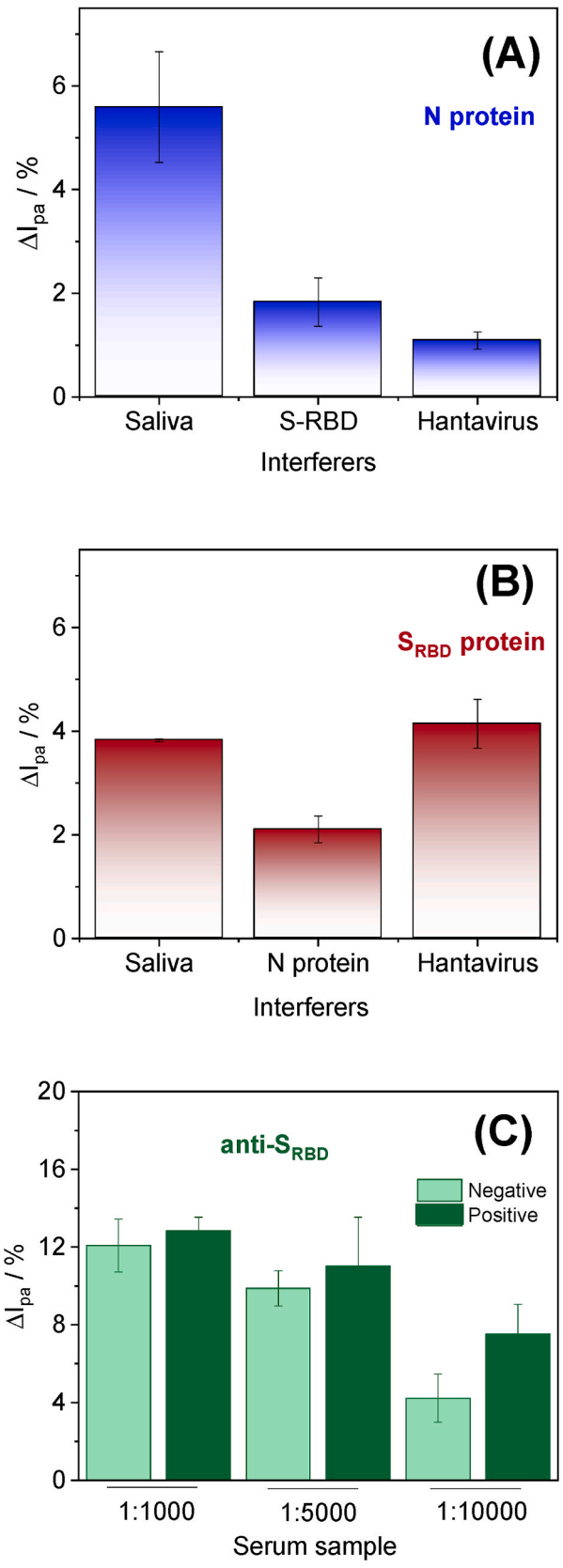

Fig. 3. Interference response of A) saliva, 500 pg mL^{-1} of S-RBD and 2 μg mL^{-1} hantavirus for the sensor prepared with N-protein receptor; B) Saliva, 500 pg mL^{-1} N-protein and 2 μg mL^{-1} hantavirus for the sensor prepared with S_{RBD} and C) serum sample of positive and negative COVID-19 controls at different dilution 1:1000, 1:5000 and 1:10,000.

3.4. Analytical performance

Multiplex detection of N, S_{RBD} proteins and anti-S_{RBD} (IgG SARs-CoV-2 antibodies) are important factors to improve the confidence levels of COVID-19 diagnostics in swab, saliva and serum samples. From this point of view, those targets were used as a proof of concept to show the promising application of the fully 3D printed multi-cell electrode to overcome clinical challenges of COVID-19 diagnoses. From this perspective, the analytical performance of the proposed sensors was investigated by cyclic voltammetry for each analyte in concentration ranges from pg to ng mL^{-1} using an external calibration. As a proof-of-concept, the calibration plots were carried out in PBS solution. The ΔI_{ap}/% is expressed by $(I_{op}\text{-}I_p/I_{op})*100$. Standard deviation for each concentration level was estimated in replicate (n = 6). Voltammograms recorded after incubation in presence of targets showed a significant variation of current peak and a small relative standard deviation (Fig. 2A, B and C).

Linear relationships between relative ΔI_{ap}/% and the logarithm of target concentrations were achieved for the three tested analytes: N protein, S_{RBD} protein and anti-S_{RBD} (Fig. 2D, E and F). The blank deviation was estimated based on the variation of the sensor response, in presence of the redox probe and PBS solution as electrolyte, before incubation step (n = 6). In those conditions, the RSD values were 4.2, 2.7 and 2.8% for N-protein, S_{RBD} and anti-S_{RBD}, respectively. The limit of detection was estimated as the first point of the calibration plot, statistically different from the blank deviation. Therefore, the LOD values were 5, 1, and 0.1 pg mL^{-1} for N protein, S_{RBD} protein and anti-S_{RBD}, respectively. Correlation coefficients were 0.986, 0.985 and 0.993 for N-protein, S_{RBD} protein and anti-S_{RBD}, respectively. Previous results showed that anti-S_{RBD} (IgG) can reach levels of μg mL^{-1} in serum 21 days after infection [22]. The levels of N protein in saliva samples can be between 10 and 10,000 pg mL^{-1} [23]. The linear response of the targets below and/or inside biological levels shows the promising features of the produced biosensors for the sequential detection and quantification of multiple COVID-19 biomarkers. Table 1 presents comparative results between COVID-19 electrochemical sensors. Compared to the voltammetric and impedimetric sensors presented on Table 1, the results indicate suitable performance of the proposed multiplex approach for the three tested targets, showing excellent limits of detection and adequate detection time for the three targets. It is important to highlight that this approach allows the simultaneous incubation of multiple targets, which is an important point for routine analysis.

3.5. Selectivity, matrix effect and multi-target determination

In order to verify the analytical applicability of the multi-analyte system, selectivity studies for N and S_{RBD} protein detection were performed in presence of a 1,000x diluted saliva from a healthy individual. Also, the interference response of other protein and virus was evaluated for those sensors. Saliva can contain high levels of N and S_{RBD} proteins being useful in the COVID-19 diagnostics. Thus, the matrix effect of diluted saliva was separately tested for the detection of N and S_{RBD} protein, showing an interference response of 5.6% and 3.8%, respectively (Fig. 3A and B). As can be seen in Fig. 3A, N-protein sensor showed an interference response of 2.2 and 1.1% in the presence of S_{RBD} (500 pg mL^{-1}) and Hantavirus (1 ng mL^{-1}), respectively. The same experiments were applied for S_{RBD} protein sensor and showed an interference response of 2.1 and 4.2% for N-protein (500 pg mL^{-1}) and Hantavirus (1 ng mL^{-1}), respectively (Fig. 3B). Those results suggest adequate selectivity for the detection of S_{RBD} and N-protein in saliva.

Since there is a significant expression of COVID-19 IgG antibodies in human blood, serological tests are the most used diagnostics for anti-S_{RBD} detection. From this perspective, the interference response of positive and negative serum samples was evaluated to achieve suitable conditions for electrochemical sensing. Both samples were diluted in PBS solution pH 7.4 in proportions of 1:1,000, 1:5,000, and 1:10,000 (v/

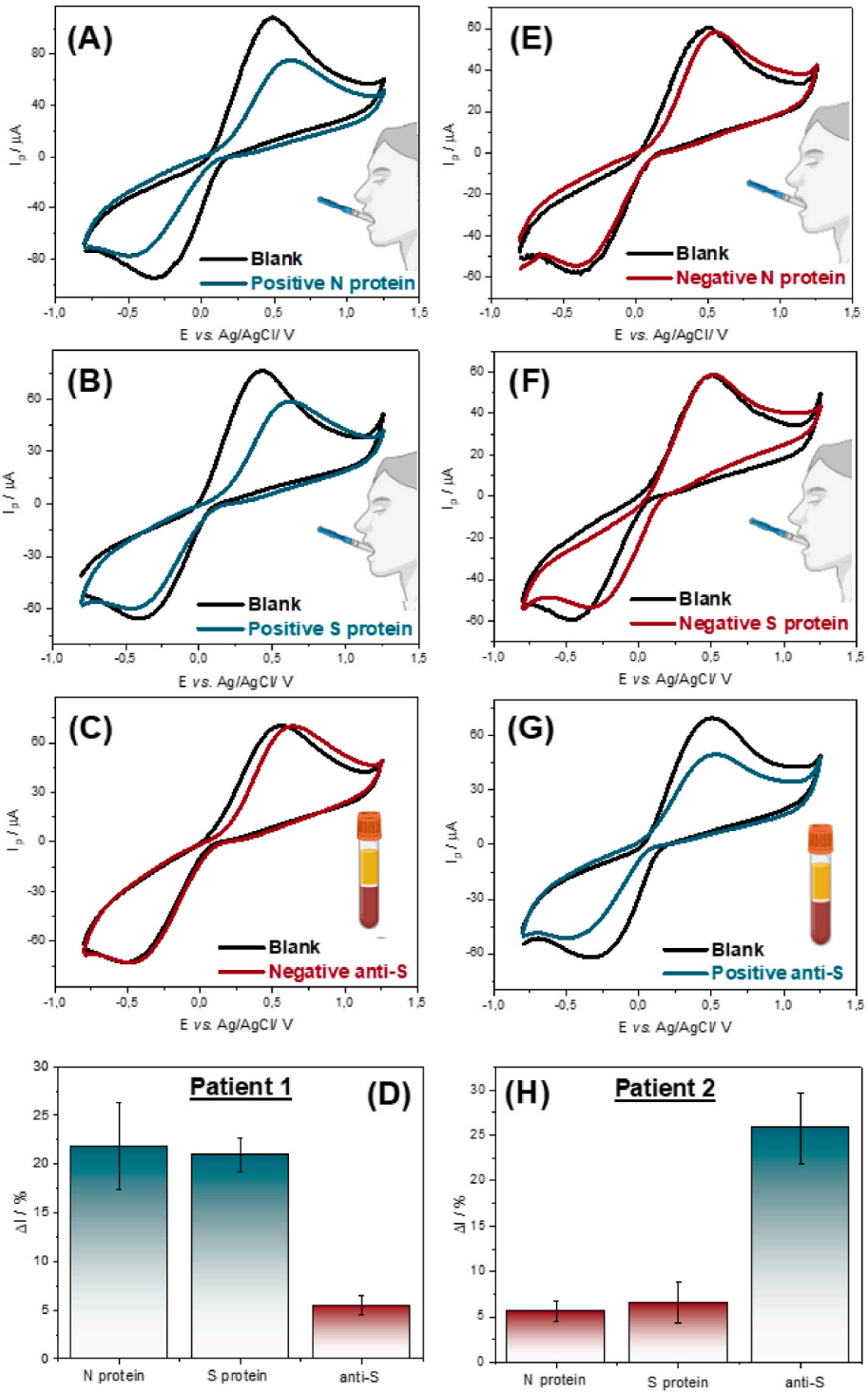

Fig. 4. Multi-analyte detection of serum and saliva spiked samples simulating two different conditions A) N protein; B) S-RBD protein; C) anti-S-RBD and D) comparative ΔI_{ap}/% for patient 1; and E) N-protein; F) S-RBD protein; G) anti-S-RBD and H) comparative ΔI_{ap}/% for patient 2.

v). As is shown in Fig. 3C, small differences of the anodic peak current, for positive and negative controls, were observed for the samples diluted 1,000x and 5,000x. It can be explained due to the high protein content and complexity of serum samples, which contributes to the non-specific binding. For the diluted 10,000x sample, the difference from positive and negative tested samples suggests appropriate conditions for selective detection of anti-S_{RBD}. Since anti-S_{RBD} serum levels are in the range of µg mL^{-1}, the proposed dilution would not compromise sensor operation for COVID-19 diagnosis. Thus, this dilution was further applied for the electrochemical multiplex detection aiming to improve the selectivity of anti-S_{RBD} in serological tests.

Multi-analyte detection is an important tool for precision diagnostics, supporting medical decision-making. Considering that, the novel multi-electrode cell was applied for multiplex detection of COVID-19 biomarkers as a proof of concept. In this particular case, despite the increasing efforts of the scientific community, there is still a wide range of false negative results, contributing to the spreading of this viral disease. It occurs because of the significant decrease in viral levels about 7

days after the first symptom. Subsequently, the organism starts to react with the production of antibodies. Considering that, multiplex detection of viral proteins and IgG antibodies could contribute to accurate diagnostics of SARS-CoV-2, increasing the detection window.

To simulate real conditions, two sets of samples were prepared, which were divided into patient 1 and patient 2. For patient 1, the saliva sample of a healthy individual was spiked simultaneously with 50 pg mL^{-1} of N and S_{RBD} proteins. Additionally, the diluted non-spiked serum of this patient 1 was analysed in the same electrochemical set-up. This condition was designed to simulate a possible patient in the early 7 days of symptoms. On the other hand, the serum of patient 2 was spiked with 50 pg mL^{-1} of anti-S_{RBD}, which was sequentially analysed with the non-spiked saliva sample. The six-working electrode cell was used in both cases. For this purpose, the electrochemical experiment was designed to present two sensors for each marker.

Fig. 4 presents the cyclic voltammograms for patients 1 and 2 performed in 5 mmol L^{-1} $K_3[Fe(CN)_6]$ in PBS pH 7.4. For patient 1, Fig. 4A, 4B, and 4C show the results for the sequential detection of N-protein, S_{RBD} protein, and anti-S_{RBD}, respectively. In those conditions, it was possible to identify a ΔI_{ap} of 21.8 (±4.5), 20.9 (±1.7), and 5.5 (±0.9) % for N-protein, S_{RBD} protein, and anti-S_{RBD}, respectively. The CV results indicate positive detection for N and S protein. On the other hand, the result was negative for anti-S_{RBD} once the produced ΔI_{ap} was lower than the first point of the calibration plot. The same experiment was applied for patient 2 and the ΔI_{ap} values were 5.6 (±1.1), 6.6 (±2.2) and 25.8 (±3.9) % for N-protein, S_{RBD} protein, and anti-S_{RBD}, respectively. Considering that, the values of N and S_{RBD} protein were also considered negative since they were lower than the first point on the calibration plot. The positive result for anti-S_{RBD} in this case indicates the selective detection of antibodies, which is suitable for multi-target sensing.

4. Conclusion

In this work, we proposed a novel 3D-printed multi-electrode portable cell for multiplex electrochemical sensing of COVID-19 biomarkers. First, the novel cell configuration was investigated to ensure its adequate operation. PLA/CB was successfully modified with graphene oxide (PLA/CB/GO), providing an adequate surface for electrochemical immunosensing. Cyclic voltammetry was employed to stepwise investigate the construction of the biosensors for N-protein, S_{RBD} protein, and anti-S_{RBD}. Under optimized conditions, it was possible to observe a linear relation between ΔI_{ap} and the logarithm of concentration for the three tested analytes. The interference response studies were also employed to estimate the adequate preparation of saliva and serum samples for multi-target detection in real samples. For multiplex sequential detection of the studied proteins, two possible conditions were simulated. The successful results of simulated samples indicate that the novel 3D-printed multi-electrode cell presents an important approach for multi-target detection using COVID-19 biomarkers as a proof of concept. This versatile 3D-printed strategy can be also used for sequential detection of other biomarkers, aiming for the precise diagnostics of infections and viral diseases. Further studies can be performed to include a high number of electrodes and biomarkers.

CRediT authorship contribution statement

Franciele de Matos Morawski: Conceptualization, Methodology, Investigation, Formal analysis, Writing – original draft. **Gustavo Martins:** Conceptualization, Methodology, Investigation, Formal analysis, editing, and reviewing the original draft. **Maria Karolina Ramos:** Formal analysis. **Aldo J.G. Zarbin:** Resources, Writing – review & editing. **Lucas Blanes:** Methodology, Funding acquisition, Resources, Writing – review & editing. **Marcio F. Bergamini:** Funding acquisition, Resources, Supervision, Project administration, Writing – review & editing. **Luiz Humberto Marcolino-Junior:** Funding acquisition, Resources, Supervision, Project administration, Writing – review & editing.

Declaration of competing interest

The authors declare that they have no known competing financial interests or personal relationships that could have appeared to influence the work reported in this paper.

Data availability

No data was used for the research described in the article.

Acknowledgments

The authors thank Coordenação de Aperfeiçoamento de Pessoal de Nível Superior (CAPES) (financial code 001 and CAPES September 2020 Epidemias 88887.504861/2020–00), Conselho Nacional de Pesquisa (CNPq) (grants 408309/2018-0; 311290/2020-5, 309803/2020-9 and 402195/2020-5) and Fundação Araucária (PBA2022011000056 and PDT2020221000003). The authors are also grateful for the technical and financial support of the Carlos Chagas Institute–FIOCRUZ/PR.

Appendix A. Supplementary data

Supplementary data to this article can be found online at https://doi.org/10.1016/j.aca.2023.341169.

References

[1] G. Nagaraju, S. Tagliaferri, A. Panagiotopoulos, M. Och, R. Quintin-Baxendale, C. Mattevi, Durable Zn-ion hybrid capacitors using 3D printed carbon composites, J. Mater. Chem. 10 (2022) 15665–15676, https://doi.org/10.1039/d2ta03488c.
[2] X. Ruan, V. Hulubei, Y. Wang, Q. Shi, N. Cheng, L. Wang, Z. Lyu, W.C. Davis, J. N. Smith, Y. Lin, D. Du, Au@PtPd enhanced immunoassay with 3D printed smartphone device for quantification of diaminochlorotriazine (DACT), the major atrazine biomarker, Biosens. Bioelectron. 208 (2022), https://doi.org/10.1016/j.bios.2022.114190.
[3] M. Shafizadeh, S. Abbasi-Moayed, Z. Hamzei, A. Keshavarz, S. Yousefi, M. R. Hormozi-Nezhad, H. Golmohammadi, Chlorophyll-based wicking sensing bioplatform coupled with a smartphone-based sample-to-answer analytical device for on-site detection of picric acid, Biosens. Bioelectron. X. 11 (2022), https://doi.org/10.1016/j.biosx.2022.100150.
[4] R.M. Cardoso, D.M.H. Mendonça, W.P. Silva, M.N.T. Silva, E. Nossol, R.A.B. da Silva, E.M. Richter, R.A.A. Muñoz, 3D printing for electroanalysis: from multiuse electrochemical cells to sensors, Anal. Chim. Acta 1033 (2018) 49–57, https://doi.org/10.1016/j.aca.2018.06.021.
[5] K.A. Deo, M.K. Jaiswal, S. Abasi, G. Lokhande, S. Bhunia, T.U. Nguyen, M. Namkoong, K. Darvesh, A. Guiseppi-Elie, L. Tian, A.K. Gaharwar, Nanoengineered ink for designing 3D printable flexible bioelectronics, ACS Nano 16 (2022) 8798–8811, https://doi.org/10.1021/acsnano.1c09386.
[6] J.L. Erkal, A. Selimovic, B.C. Gross, S.Y. Lockwood, E.L. Walton, S. McNamara, R. S. Martin, D.M. Spence, 3D printed microfluidic devices with integrated versatile and reusable electrodes, Lab Chip 14 (2014) 2023–2032, https://doi.org/10.1039/c4lc00171k.
[7] M.F. Santangelo, S. Libertino, A.P.F. Turner, D. Filippini, W.C. Mak, Integrating printed microfluidics with silicon photomultipliers for miniaturised and highly sensitive ATP bioluminescence detection, Biosens. Bioelectron. 99 (2018) 464–470, https://doi.org/10.1016/j.bios.2017.07.055.
[8] S.M. Sibug-Torres, L.P. Go, V.C.G. Castillo, J.L.R. Pauco, E.P. Enriquez, Fully integrated 3D-printed electrochemical cell with a modified inkjet-printed Ag electrode for voltammetric nitrate analysis, Anal. Chim. Acta 1160 (2021), https://doi.org/10.1016/j.aca.2021.338430.
[9] A.F. João, L.V. de Faria, D.L.O. Ramos, R.G. Rocha, E.M. Richter, R.A.A. Muñoz, 3D-printed carbon black/polylactic acid electrochemical sensor combined with batch injection analysis: a cost-effective and portable tool for naproxen sensing, Microchem. J. 180 (2022), https://doi.org/10.1016/j.microc.2022.107565.
[10] C. Kalinke, P.R. de Oliveira, B.C. Janegitz, J.A. Bonacin, Prussian blue nanoparticles anchored on activated 3D printed sensor for the detection of L-cysteine, Sensor. Actuator. B Chem. 362 (2022), https://doi.org/10.1016/j.snb.2022.131797.
[11] L.R.G. Silva, J.S. Stefano, L.O. Orzari, L.C. Brazaca, E. Carrilho, L.H. Marcolino-Junior, M.F. Bergamini, R.A.A. Munoz, B.C. Janegitz, Electrochemical biosensor for SARS-CoV-2 cDNA detection using AuPs-modified 3D-printed graphene electrodes, Biosensors 12 (2022), https://doi.org/10.3390/bios12080622.
[12] J.S. Stefano, C. Kalinke, R.G. Da Rocha, D.P. Rocha, V.A.O.P. Da Silva, J. A. Bonacin, L. Angnes, E.M. Richter, B.C. Janegitz, R.A.A. Muñoz, Electrochemical (Bio)Sensors enabled by fused deposition modeling-based 3D printing: a guide to selecting designs, printing parameters, and post-treatment protocols, Anal. Chem. 94 (2022) 6417–6429, https://doi.org/10.1021/acs.analchem.1c05523.

[13] L. Krejcova, L. Nejdl, M.A.M. Rodrigo, M. Zurek, M. Matousek, D. Hynek, O. Zitka, P. Kopel, V. Adam, R. Kizek, 3D printed chip for electrochemical detection of influenza virus labeled with CdS quantum dots, Biosens. Bioelectron. 54 (2014) 421–427, https://doi.org/10.1016/j.bios.2013.10.031.

[14] G. Martins, J.L. Gogola, L.H. Budni, B.C. Janegitz, L.H. Marcolino-Junior, M. F. Bergamini, 3D-printed electrode as a new platform for electrochemical immunosensors for virus detection, Anal. Chim. Acta 1147 (2021) 30–37, https://doi.org/10.1016/j.aca.2020.12.014.

[15] D. Najjar, J. Rainbow, S. Sharma Timilsina, P. Jolly, H. de Puig, M. Yafia, N. Durr, H. Sallum, G. Alter, J.Z. Li, X.G. Yu, D.R. Walt, J.A. Paradiso, P. Estrela, J.J. Collins, D.E. Ingber, A lab-on-a-chip for the concurrent electrochemical detection of SARS-CoV-2 RNA and anti-SARS-CoV-2 antibodies in saliva and plasma, Nat. Biomed. Eng. 6 (2022) 968–978, https://doi.org/10.1038/s41551-022-00919-w.

[16] B. Van Dang, A. Hassanzadeh-Barforoushi, M.S. Syed, D. Yang, S.J. Kim, R. A. Taylor, G.J. Liu, G. Liu, T. Barber, Microfluidic actuation via 3D-printed molds toward multiplex biosensing of cell apoptosis, ACS Sens. 4 (2019) 2181–2189, https://doi.org/10.1021/acssensors.9b01057.

[17] F. Jiang, Z. Xiao, T. Wang, J. Wang, L. Bie, L. Saleh, K. Frey, L. Zhang, J. Wang, Rapid and sensitive multiplex detection of COVID-19 antigens and antibody using electrochemical immunosensor-/aptasensor-enabled biochips, Chem. Commun. 58 (2022) 7285–7288, https://doi.org/10.1039/d2cc01598f.

[18] I. Sampaio, F.D. Quatroni, J.N. Yamauti Costa, V. Zucolotto, Electrochemical detection of Zika and Dengue infections using a single chip, Biosens. Bioelectron. 216 (2022), https://doi.org/10.1016/j.bios.2022.114630.

[19] N.I. Zaaba, K.L. Foo, U. Hashim, S.J. Tan, W.W. Liu, C.H. Voon, Synthesis of graphene oxide using modified hummers method: solvent influence, Procedia Eng. 184 (2017) 469–477, https://doi.org/10.1016/j.proeng.2017.04.118.

[20] E.M. Richter, D.P. Rocha, R.M. Cardoso, E.M. Keefe, C.W. Foster, R.A.A. Munoz, C. E. Banks, Complete additively manufactured (3D-printed) electrochemical sensing platform, Anal. Chem. 91 (2019) 12844–12851, https://doi.org/10.1021/acs.analchem.9b02573.

[21] A. Yakoh, U. Pimpitak, S. Rengpipat, N. Hirankarn, O. Chailapakul, S. Chaiyo, Paper-based electrochemical biosensor for diagnosing COVID-19: detection of SARS-CoV-2 antibodies and antigen, Biosens. Bioelectron. 176 (2021), https://doi.org/10.1016/j.bios.2020.112912.

[22] H. Ma, W. Zeng, H. He, D. Zhao, Y. Yang, D. Jiang, P. Zhou, Y. Qi, W. He, C. Zhao, R. Yi, X. Wang, B. Wang, Y. Xu, Y. Yang, A.J.K. Kombe, C. Ding, J. Xie, Y. Gao, L. Cheng, Y. Li, X. Ma, T. Jin, COVID-19 diagnosis and study of serum SARS-CoV-2 specific IgA, IgM and IgG by a quantitative and sensitive immunoassay, medRxiv (2020), 2020.04.17.20064907.

[23] D. Shan, J.M. Johnson, S.C. Fernandes, H. Suib, S. Hwang, D. Wuelfing, M. Mendes, M. Holdridge, E.M. Burke, K. Beauregard, Y. Zhang, M. Cleary, S. Xu, X. Yao, P. P. Patel, T. Plavina, D.H. Wilson, L. Chang, K.M. Kaiser, J. Nattermann, S. V. Schmidt, E. Latz, K. Hrusovsky, D. Mattoon, A.J. Ball, N-protein presents early in blood, dried blood and saliva during asymptomatic and symptomatic SARS-CoV-2 infection, Nat. Commun. 12 (2021), https://doi.org/10.1038/s41467-021-22072-9.

[24] G. Martins, J.L. Gogola, L.H. Budni, M.A. Papi, M.A.T. Bom, M.L.T. Budel, E.M. De Souza, M. Müller-santos, B.C.B. Beir, Novel approach based on GQD-PHB as anchoring platform for the development of SARS-CoV-2 electrochemical immunosensor, Anal. Chim. Acta 1232 (2022), 340442, https://doi.org/10.1016/j.aca.2022.340442.

[25] A.R. Cardoso, J.F. Alves, M.F. Frasco, A.M. Piloto, V. Serrano, D. Mateus, A. I. Sebastião, A.M. Matos, A. Carmo, T. Cruz, E. Fortunato, M.G.F. Sales, An ultra-sensitive electrochemical biosensor using the Spike protein for capturing antibodies against SARS-CoV-2 in point-of-care, Mater. Today Bio. 16 (2022), https://doi.org/10.1016/j.mtbio.2022.100354.

[26] S. Ramanathan, S.C.B. Gopinath, Z.H. Ismail, M.K. Md Arshad, P. Poopalan, Aptasensing nucleocapsid protein on nanodiamond assembled gold interdigitated electrodes for impedimetric SARS-CoV-2 infectious disease assessment, Biosens. Bioelectron. 197 (2022), 113735, https://doi.org/10.1016/j.bios.2021.113735.

[27] L. Fabiani, M. Saroglia, G. Galatà, R. De Santis, S. Fillo, V. Luca, G. Faggioni, N. D'Amore, E. Regalbuto, P. Salvatori, G. Terova, D. Moscone, F. Lista, F. Arduini, Magnetic beads combined with carbon black-based screen-printed electrodes for COVID-19: a reliable and miniaturized electrochemical immunosensor for SARS-CoV-2 detection in saliva, Biosens. Bioelectron. 171 (2021), https://doi.org/10.1016/j.bios.2020.112686.

[28] A. Roberts, S. Mahari, D. Shahdeo, S. Gandhi, Label-free detection of SARS-CoV-2 Spike S1 antigen triggered by electroactive gold nanoparticles on antibody coated fluorine-doped tin oxide (FTO) electrode, Anal. Chim. Acta 1188 (2021), 339207, https://doi.org/10.1016/j.aca.2021.339207.

[29] M. Amouzadeh Tabrizi, J.P. Fernández-Blázquez, D.M. Medina, P. Acedo, An ultrasensitive molecularly imprinted polymer-based electrochemical sensor for the determination of SARS-CoV-2-RBD by using macroporous gold screen-printed electrode, Biosens. Bioelectron. 196 (2022), https://doi.org/10.1016/j.bios.2021.113729.

[30] E.B. Aydın, M. Aydın, M.K. Sezgintürk, Highly selective and sensitive sandwich immunosensor platform modified with MUA-capped GNPs for detection of spike Receptor Binding Domain protein: a precious marker of COVID 19 infection, Sensor. Actuator. B Chem. 345 (2021), 130355, https://doi.org/10.1016/j.snb.2021.130355.

[31] E. Karakus, E. Erdemir, N. Demirbilek, L. Liv, Colorimetric and electrochemical detection of SARS-CoV-2 spike antigen with a gold nanoparticle-based biosensor, Anal. Chim. Acta 1182 (2021), 338939, https://doi.org/10.1016/j.aca.2021.338939.